Elasticity of dilatant particle suspensions during flow

Ryan J. Larsen,[1,2] Jin-Woong Kim,[1,*] Charles F. Zukoski,[2] and David A. Weitz[1,3]
[1]*School of Engineering and Applied Sciences, Harvard University, 29 Oxford Street, Cambridge, Massachusetts 02138, USA*
[2]*Department of Biomolecular and Chemical Engineering, University of Illinois at Urbana–Champaign, 114 Roger Adams Laboratory, 600 South Mathews, Urbana, Illinois 61801, USA*
[3]*Department of Physics, Harvard University, 29 Oxford Street, Cambridge, Massachusetts 02138, USA*
(Received 9 January 2009; revised manuscript received 8 November 2009; published 20 January 2010)

Dense suspensions under sufficiently high shear stress can exhibit a dramatic transition to a solidlike state. This is known as extreme shear thickening and is sometimes accompanied by dilatancy. This behavior is contradictory; the material is solidlike but only when flowing. To probe the elasticity of the dilatant state, we measure the transient inertio-elastic oscillations that occur in response to step changes in applied stress. As the volume fraction of solids increases the apparent flow elasticity also increases, and the suspension flows more slowly, approaching an elastic solid, which will support stress statically.

DOI: 10.1103/PhysRevE.81.011502 PACS number(s): 83.50.−v, 83.80.Hj, 83.60.Df, 83.60.Rs

I. INTRODUCTION

Many dense suspensions exhibit a dramatic yet reversible increase in viscosity when subjected to sufficiently high stress. This effect can be so severe that it can damage machinery and even enhance the ballistic impact resistance of armor [1]. One form of thickening occurs when the applied stress overcomes the repulsive forces between particles, causing them to form "hydroclusters" which drive the viscosity increase [2]. Stokesian dynamics simulations predict a negative first normal stress difference, N_1, [3] and this characteristic feature has been confirmed experimentally [4]. A distinct class of thickening occurs in suspensions during extreme shear thickening characterized by positive N_1; this reflects dilatancy [5–7]. Perhaps the best known example of this behavior is cornstarch in water [6]. Dilatant suspensions accommodate flow by expanding under shear: the outermost particles are pushed against the liquid interface to provide more free volume to the internal particles [8]. Dilatancy gives rise to solidlike behavior that cannot be described by the fluidlike behavior associated with hydroclusters. These effects tend to occur at elevated volume fractions and are associated with particle crowding or jamming [7,9–13].

The solidlike nature of suspensions undergoing extreme thickening has been difficult to characterize. Flow elasticity can be measured during continuous gradual shear thickening using a stress superposition technique, but this is difficult to interpret [14]. As a result, little is known about the combination of liquidlike and solidlike behavior essential to describing dilatant flows of suspensions.

In this paper, we report measurements of shear rate fluctuations associated with dilatant materials during flow resolved to millisecond time scales. We observe elastic recoil upon cessation of shear, demonstrating that the suspensions can store stresses elastically [15]. We also observe transient fluctuations in the strain rate following step increases in stress, similar to the inertio-elastic oscillations observed in elastic materials [16]. The frequency of the inertio-elastic oscillations provides a measure of sample elasticity even as the sample is flowing [16]. We apply this analysis to dilatant suspensions and show that the apparent elasticity increases with the particle volume fraction. We rationalize our results with a physical picture in which the solidlike characteristics are caused by clusters of particles that store stress elastically. The presence of these clusters within the liquid allows it to flow like a viscous liquid, while simultaneously storing energy like an elastic solid.

II. METHODS

Our experiments were performed on polystyrene particles synthesized using a seeded polymerization technique [11]. After synthesis, the particles were washed in methanol and then dispersed into an aqueous solution containing 0.05 wt % Pluronic® F-68 surfactant (Fluka). We made two batches of spherical particles ($S1$ and $S2$) and two batches of dumbbell-shaped particles ($D1$ and $D2$). Analysis of images obtained by scanning electron microscopy revealed the radius, a, of the $S1$ and $S2$ particles to be 2.9 μm, while the dumbbells particles consist of two interpenetrating spheres, each of radius 1.9 and 2.0 μm for $D1$ and $D2$, respectively. The displacements between the spheres are 1.8 and 1.7 μm, respectively, thus the particle volumes are equivalent to those occupied by spheres of radius 2.2 and 2.3 μm, for $D1$ and $D2$, respectively. Rheological properties were measured at 25 °C using AR-G2 rheometers (TA Instruments, New Castle, USA) equipped with 40 mm parallel plates mounted with homemade paralene-coated aluminum plates roughened to reduce slip. To ensure maximum reproducibility, samples were carefully loaded into the rheometer. This was done by using a spatula to place the sample onto the lower plate and then slowly lowering the upper plate until the sample was flush with the edges. No excess sample was removed because this tended to give rise to rheological behavior that exhibited more solidlike behavior. For all experiments in which we compare results between different samples, we attempted to load a sample quantity that would correspond to a gap height close to 1000 μm. In practice, the gap heights tended to

*Present address: Amore Pacific R&D Ctr, Yongin 446729, Gyeonggi Do, South Korea.

vary somewhat but were always within the range of 800–1200 μm. After loading the samples, we performed tests at constant torque or stress, σ. The resulting rate of rotation of the rheometer is proportional to the average shear rate of the sample, from which we calculate an apparent viscosity, η. After loading the sample, we applied a series of ascending, and then descending, stresses, between 0.1 and 45 Pa. Even after careful sample loading, values of η measured during the initial experiments of ascending stress steps tended to be greater than those measured during the subsequent experiments of descending stress steps. For most samples, this discrepancy was only observed during the first series of ascending and descending stress tests. The descending stress steps from the fist series of measurements after loading tended to establish values of η that were precisely matched by subsequent ascending and descending flow curves. After establishing this reproducible state, we performed oscillatory strain sweeps to characterize the linear viscoelastic properties of the suspension. Next we performed experiments in which the stress was stepped from 0.1 Pa to higher stress values in the range of 200–400 Pa. We then performed additional measurements at the elevated stresses with a series of constant stress tests that alternated in regular patterns between σ=200, 400, and 600 Pa. A detailed analysis of the results from these experiments is the focus of this paper. Finally, we repeated the ascending and descending stress steps between 0.1 and 45 Pa to assure that no significant drift had occurred in the sample properties. Measured values of η had generally not increased by more than a factor of two at the conclusion of the experiments. This indicates that the shear thickening effects studied here are mostly reversible especially for the dumbbell particles. The samples that were the least reversible were the spherical particles of highest volume fraction. With these samples, we consistently observed discrepancies between ascending and descending flow curves between 0.1 and 45 Pa. Nevertheless, we still performed experiments at elevated stress levels on these samples, and we include these results in the data presented here.

During our experiments, we monitored the fluctuations in the flow by collecting angular displacement and torque data from the rheometer at a rate of 1000 points/s. During the normal force measurements, the rate of data collection was reduced to 250 points per second to allow for collection of the additional data. Instantaneous shear rates, $\dot{\gamma}$, were calculated from a simple backward derivative of the strain with no smoothing applied.

III. RESULTS

We investigated suspension volume fractions, ϕ, above 0.57, where the suspensions had linear viscoelastic responses, with the elastic modulus greater than the viscous modulus, and typical elastic moduli between 0.1 and 1 Pa when probed with strain-controlled oscillations at 1 rad/s. As the strain amplitude increased, the suspensions typically yielded at strains around 0.1, corresponding to typical yield stresses between 0.01 and 0.1 Pa.

The viscous properties at higher stresses were measured with step stress tests. The basic trends in $\eta(\sigma)$ are similar for

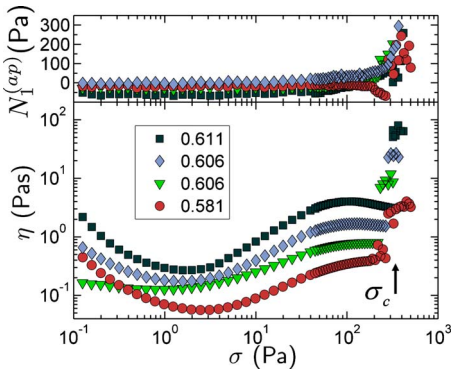

FIG. 1. (Color online) Both $N_1^{(ap)}$ and η show dramatic increases when $\sigma > \sigma_c$. For the $D1$ samples shown here, $\sigma_c \approx 200–300$ Pa. Both spheres and dumbbells showed qualitatively similar flow curves.

all measured volume fractions: at low stresses, η decreases with increasing applied stress, reflecting shear-thinning behavior. As the stress increases further, η increases, reflecting shear-thickening behavior, and then reaches a plateau, as shown for the $D1$ samples in the lower panel of Fig. 1. This is followed by a dramatic increase in η at a high characteristic stress, σ_c, typically between 50 and 300 Pa, as shown by the arrow in Fig. 1. This sudden increase in η corresponds to a simultaneous increase in the normal force, f, that is measured by a strain gauge located beneath the lower stationary plate. We convert f to an apparent first normal stress difference, $N_1^{(ap)} = 2f/\pi R^2$, where R is the radius of the plate, and neglecting the N_2 contribution, which is small in dilatant systems [6]. The positive values of $N_1^{(ap)}$ for $\sigma > \sigma_c$ indicate that the suspension tends to push the parallel plates apart (Fig. 1). This separating force is caused by particles that dilate against the bounding surfaces to accommodate flow [6,7]. At high stresses, we also observed tearing or cracking on the liquid interface during our experiments. In some of samples of highest ϕ, solidlike particle clusters churned out from between the plates [17]. This behavior is also consistent with dilatancy [6].

The dilatant suspensions are able to store stresses that persist even after the cessation of flow [15]. This property is apparent at the end of the steady stress test shown in Fig. 1 on the $D1$ sample at ϕ=0.611. At the moment when σ drops to zero, the sample abruptly reverses the direction of rotation, which briefly rotates slightly more quickly in the "negative" direction than it had previously been rotating under σ =445 Pa as shown in Fig. 2. The energy necessary for this reversal of direction must be supplied by elastic stress stored in the sample during dilatant flow.

The elastic behavior is not likely to originate from entropic effects; the magnitude of the entropic stresses is set by kT/a^3, which is approximately 10^{-4} of σ_c. A second possible source of elasticlike behavior is related to the air/water interface. The surface tension of the water opposes the stress-induced expansion of dilatant particle clusters. These clusters can cause particles to protrude against the air/water interface, thereby increasing its surface area and giving it a matted appearance [8]. When the applied stress vanishes, the energy that was stored in the new air/water interface is dissipated as

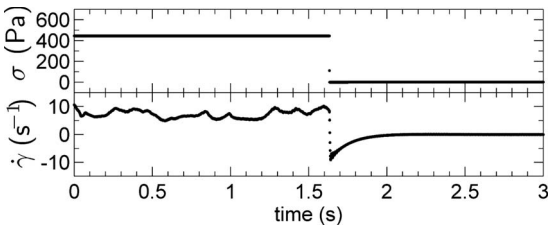

FIG. 2. At the end of the steady stress tests on sample of $D1$, $\phi=0.611$, the rheometer reverses direction due to elasticity in the sample.

the particles return to the bulk and the liquid recovers its glossy appearance. This mechanism can therefore account for energy storage and subsequent dissipation and may therefore be responsible for elasticlike effects. However, it is unlikely that this mechanism is responsible for the observed elastic recoil because the particle recoil from the interface will only push the particles in the direction that is radial with respect to the upper plate. By contrast, the recoil observed in our experiments is in the direction of rotation. We therefore conclude that the most likely cause of the elastic recoil is either the repulsive forces between particles in stress-induced clusters or the elasticity associated with individual particles [13,18,19].

To measure the elastic properties of suspensions during dilatancy, we designed a series of experiments that could probe the sample rapidly, thereby decreasing the likelihood of sample loss or irreversible cluster formation. We applied a series of step changes in applied stress, all above σ_c. Step stresses were applied in a regular sequence, such as that shown in Fig. 3(a). Each step pattern was repeated four to six times to ensure that any differences in the step-stress responses are due to the applied stress rather than to time-dependent changes in the sample, such as loss of material or irreversible particle aggregation. The flow during the stress step tests is characterized by significant fluctuations, of standard deviation $\Delta\dot{\gamma}$, about a mean shear rate, $\bar{\dot{\gamma}}$, as shown in Fig. 3(c) [20]. Values of $\bar{\dot{\gamma}}$ are independent of the applied

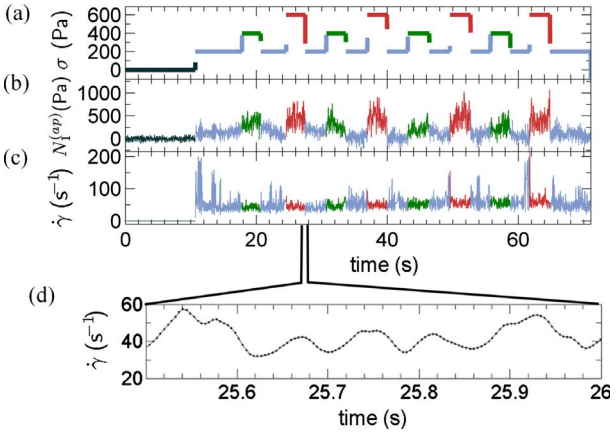

FIG. 3. (Color online) Step stress pattern on sample $S1$, $\phi=0.583$. Values of $N_1^{(ap)}$ are proportional to σ, even as $\bar{\dot{\gamma}}$ and $\Delta\dot{\gamma}$ remain constant, with the exception of occasional high shear rates at 200 Pa.

stress σ, consistent with the discontinuous shear thickening observed with steady stress measurements; surprisingly $\Delta\dot{\gamma}$ values are also independent of σ, except for samples at the lowest ϕ, and at the lowest stress, $\sigma=200$ Pa, where the fluctuations are sometimes punctuated by temporary increases to large shear rates, as seen in Fig. 3(c). A full analysis of these fluctuations is beyond the scope of this paper; here we analyze only the data corresponding to $\sigma\geq 400$ Pa, where the large fluctuations are rarely observed.

Although increasing σ in dilatant regime fails to increase both $\bar{\dot{\gamma}}$ and $\Delta\dot{\gamma}$, it does cause an increase in $N_1^{(ap)}$, as shown in Fig. 3(b). A single value of $N_1^{(ap)}$ was reported by the rheometer software during each stress step; these values are proportional to σ. We calculated the proportionality constants associated with each sample and then averaged these values from all the samples made from each batch of particles. The averaged values are 0.7, 0.6, 0.4, and 1.3 for the $S1$, $S2$, $D1$, and $D2$ batches, respectively [5]. Values of $N_1^{(ap)}$ are therefore of the same magnitude as σ, suggesting that during dilatancy the suspension is able to support shear stress due to solidlike contacts between particles.

To measure the apparent elasticity during the flow, we observe transient $\dot{\gamma}$ oscillations immediately following step changes in stress. These transients show damped, oscillatory ringing patterns, as expected for viscoelastic materials [16,21,22]. In general, these oscillations result from a periodic exchange of energy between the rotational kinetic energy of the rheometer and the elastic strain energy of the sample. In these circumstances the frequency of the inertio-elastic "ringing" is determined by a balance between the rheometer inertia and the sample elasticity and can therefore provide a measure the elasticity of the sample even during flow [16]. Elastic properties are typically extracted from transient oscillations by comparing them to the oscillations predicted by a simple rheological models [16]. We therefore extract values of an apparent flow elasticity, G, from our data by fitting the observed transient response to that predicted by a simple Maxwell model.

In this analysis, fluctuations in the stress, σ_S, that is carried by the sample are balanced by the inertial term in the equation of motion that governs the rotation of the rheometer

$$a\ddot{\gamma}+\sigma_S=\sigma. \tag{1}$$

In this expression, a is proportional to the rotational inertia, I, of the rheometer

$$a=IF_\sigma/F_\gamma, \tag{2}$$

where F_σ and F_γ are the standard conversion factors for converting torque and displacement of the rheometer to stress and strain, respectively. In the Maxwell model, σ_S is supported by an elastic element of stiffness G in series with a viscous element of viscosity η_2. The strains of the elastic and viscous elements are given by γ_1 and γ_2, respectively, and the stresses are given by $G\gamma_1$ and $\eta_2\dot{\gamma}_2$, respectively. Therefore, $\sigma_S=G\gamma_1=\eta_2\dot{\gamma}_2$ and $\gamma=\gamma_1+\gamma_2$. Using an ODE solver on MATLAB® software, we numerically solve Eq. (1) for γ and its derivatives beginning at the time when the stress step is imposed, taken to be $t=0$, subject to the initial conditions

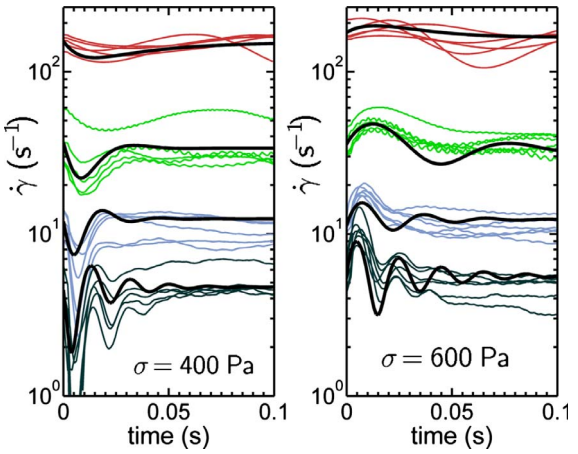

FIG. 4. (Color online) Shear rate transients from sample $D1$ during alternating stress steps between 400 and 600 Pa. The heavy black lines show solutions of the Maxwell model, using representative values of G, η_2, and γ_{10} as described in the text. Samples are the same as those shown in Fig. 1. Ascending from the low shear rates, they are ϕ=0.611, G=9300 (gray or darkest thin lines); ϕ=0.606, G=5000 (blue or lightest thin lines); ϕ=0.606, G=1500 (green or second lightest thin lines); and ϕ=0.581, G=400 Pa (red or third lightest thin lines).

$$\dot{\gamma}|_{t=0} = \dot{\gamma}_0, \tag{3a}$$

$$\gamma_1|_{t=0} = \gamma_{10}, \tag{3b}$$

$$\gamma_2|_{t=0} = 0. \tag{3c}$$

Values of $\dot{\gamma}_0$ are determined from the experiments and values of η_2 are determined from the average shear rate during the transient region, usually taken to be about 0.1–0.5 s after the stress step. Values of G and γ_{10} are used as fitting parameters in an optimization routine that solves the differential equation iteratively, finding values of γ_{10}, and G that minimize the least-squares difference between the Maxwell model prediction and the transient shear rate data. Samples that exhibited the extremely large shear rate fluctuations were excluded from the analysis.

We first performed this analysis on each of the transient responses of the $D1$ sample that are shown in Fig. 4. To produce the heavy lines in Fig. 4, we averaged the values of G, η_2, and γ_{10} that were obtained from the fits to each transient response, with some outliers excluded. Comparison between the data and model shows that the Maxwell model captures the qualitative features of the transients and many of the quantitative features: the frequency of the shear rate oscillations increases with volume fraction. This experimental observation is reflected in the fact that the apparent flow elasticity, G, increases with increasing ϕ. These results demonstrate that the Maxwell model provides a method for relating differences in transient $\dot{\gamma}$ behavior to a characteristic and apparent flow modulus, G.

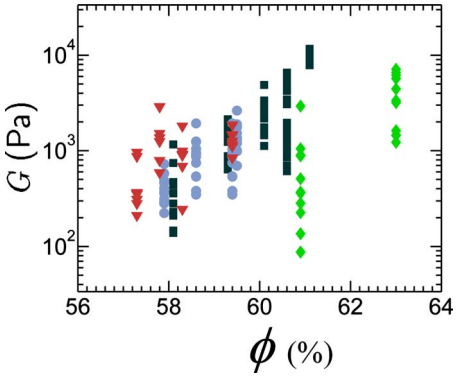

FIG. 5. (Color online) As the volume fraction, ϕ, increases the flow elasticity, G, increases for $S1$ (red triangles), $S2$ (blue circles), $D1$ (black squares), and $D2$ (green diamonds). Each symbol is calculated from a single stress step at either 400 or 600 Pa.

A. Volume fraction dependence

Measured values of G increase with increasing ϕ for all samples, as shown in Fig. 5. Increasing ϕ also causes both $\bar{\dot{\gamma}}$ and $\Delta\dot{\gamma}$ to decrease (Fig. 6). Therefore, G and $\bar{\dot{\gamma}}$ exhibit an inverse relationship (Fig. 7). As $\bar{\dot{\gamma}}$ and $\Delta\dot{\gamma}$ decrease, the ratio $\Delta\dot{\gamma}/\bar{\dot{\gamma}} \approx 0.2$ remains independent of ϕ (Fig. 8). This implies that even under the most solidlike conditions any flow is inherently unstable: no flow is possible without fluctuations.

Flow fluctuations are coupled to the stress in the sample, σ_S, according to Eq. (1). If, at a given moment, the sample cannot support the applied stress, σ, then the rheometer must accelerate. Rheometer acceleration will give rise to progressively higher values of $\dot{\gamma}$. Higher shear rates induce more solidlike structures in the sample. Subsequent deceleration of the rheometer will occur only when these structures are capable sustaining an elevated sample stress, $\sigma_S > \sigma$. When this occurs, values of $\dot{\gamma}$ will decrease. At lower $\dot{\gamma}$ the stress-bearing structures in the sample are no longer capable of supporting σ, and the cycle begins again. Therefore, mea-

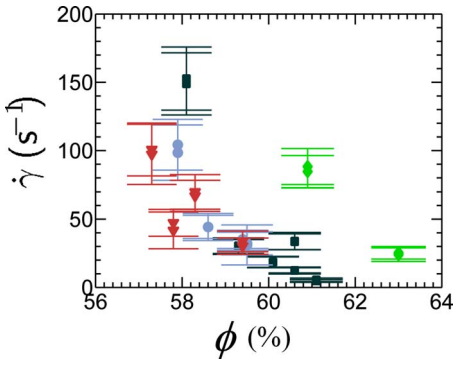

FIG. 6. (Color online) As the volume fraction, ϕ, increases the mean shear rate, $\bar{\dot{\gamma}}$, and shear rate fluctuation amplitude, $\Delta\dot{\gamma}$, decrease. Symbols correspond to $\bar{\dot{\gamma}}$, and the bars show one standard deviation, $\Delta\dot{\gamma}$, calculated from the combined shear rate data from all stress steps, with separate symbols used for 400 and 600 Pa. Symbols represent $S1$ (red triangles), $S2$ (blue circles), $D1$ (black squares), and $D2$ (green diamonds).

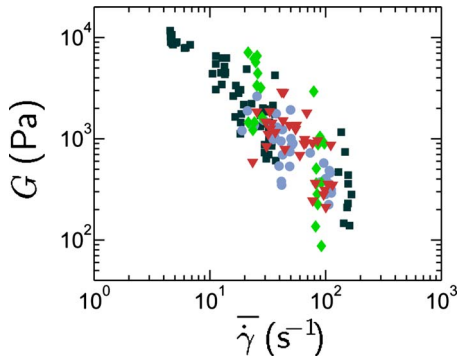

FIG. 7. (Color online) As the mean shear rate, $\bar{\dot{\gamma}}$, decreases, the flow elasticity, G, increases for $S1$ (red triangles), $S2$ (blue circles), $D1$ (black squares), and $D2$ (green diamonds). Each symbol is calculated from a single stress step at either 400 or 600 Pa.

surements of the magnitude of the fluctuations in σ_S provide information about how effective the stress-bearing structures are in supporting σ in a continuous fashion.

We calculate the time dependence of σ_S during the fluctuations using the equation of motion for the rheometer [Eq. (1)]. We calculate $\ddot{\gamma}$ by taking a second derivative of the raw displacement data. This was done by taking a backward difference derivative of the $\dot{\gamma}$ data that was first calculated with a simple backward derivative and then smoothed with a Savitzky-Golay algorithm available in MATLAB®. We verified the accuracy of this approach by calculating σ_s during the transients in $\dot{\gamma}$ following step stress changes on a Newtonian calibration oil. The calculated σ_s were found to be proportional to $\dot{\gamma}$ at all times. The constant of proportionality was equal to the viscosity of the liquid, confirming that we can accurately measure sample stresses over millisecond time scales and during transient responses when inertial stresses are important.

We quantify the magnitude of the fluctuations in inertial stress by calculating the standard deviation, $\Delta\sigma_s$, of σ_s values observed during the step stress tests. Values of $\Delta\sigma_s$ decrease with $\bar{\dot{\gamma}}$, as shown in Fig. 9. Low values of $\Delta\sigma_s$ are observed when the materials are more solidlike. As the samples become more solidlike, the stress-bearing structures are more likely to be able to support σ at any given moment, thereby preventing significant rheometer acceleration and the associated fluctuations in $\Delta\sigma_s$.

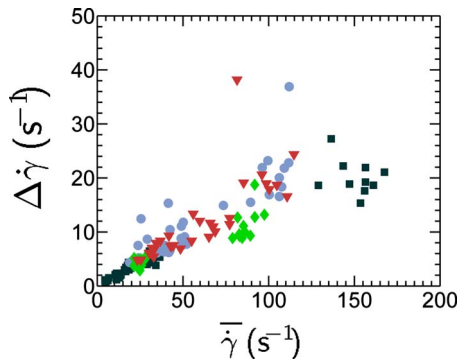

FIG. 8. (Color online) As the mean shear rate, $\bar{\dot{\gamma}}$, decreases, the shear rate fluctuation amplitude, $\Delta\dot{\gamma}$, also decreases for $S1$ (red triangles), $S2$ (blue circles), $D1$ (black squares), and $D2$ (green diamonds). Each symbol is calculated from a single stress step at either 400 or 600 Pa.

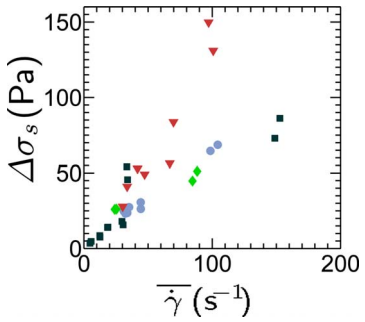

FIG. 9. (Color online) The standard deviation of σ_s is an increasing function of the mean shear rate, $\bar{\dot{\gamma}}$. Each symbol corresponds to statistics calculated from all stress steps at a given stress, (σ=400 Pa or σ=600 Pa) performed on a single sample. Symbols represent $S1$ (red triangles), $S2$ (blue circles), $D1$ (black squares), and $D2$ (green diamonds).

We expect that if we were able to increase ϕ further, then at some critical value, ϕ_c, the stress-bearing structures would be able support σ in a continuous fashion. At this point, the stress-bearing structures are stable, no flow fluctuations are present, and $\Delta\bar{\dot{\gamma}}=\dot{\gamma}=0$. When $\dot{\gamma}=0$, there are no viscous mechanisms available for stress dissipation; stresses must therefore be stored in the sample. In this state the material is solidlike and would be expected to exhibit a yield stress that exceeds 600 Pa [9]. A rough estimate of ϕ_c is obtained by linear fits to both $\bar{\dot{\gamma}}$ and $\Delta\dot{\gamma}$ as functions of ϕ. Both measures show excellent agreement, with ϕ_c=0.60, 0.60, 0.61, and 0.64 for $S1$, $S2$, $D1$, and $D2$, respectively. Our results suggests that ϕ_c of the dumbbells may be slightly higher than that of the spheres, perhaps due to more efficient packing of the slightly nonspherical shapes [23].

B. Gap height dependence

If G is indeed a material property, it is reasonable to expect that it should be independent of the gap height, d. To probe the dependence of G on d, we repeated the stress step measurements on sample $S1$ at ϕ=0.58, with the rheometer set at various gap heights: 550, 750, 950, and 1250 μm. Fits to the transient responses following the step stresses show that G is roughly independent of d [Fig. 10(a)]. From the calculated G values we characterize the frequency, f, of the transient shear rate oscillations using a standard equation for the Maxwell model [16]

$$f=\left(\frac{G}{a}-\frac{G^2}{4\eta_2^2}\right)^{1/2}/2\pi. \tag{4}$$

The parameter, a, in this equation is inversely proportional to F_γ which, for a parallel-plate rheometer, is inversely proportional to d [see Eq. (2)]. The leading term of Eq. (4) therefore predicts that for a fixed G, values of f should increase as d decreases. This is shown in Fig. 10(b).

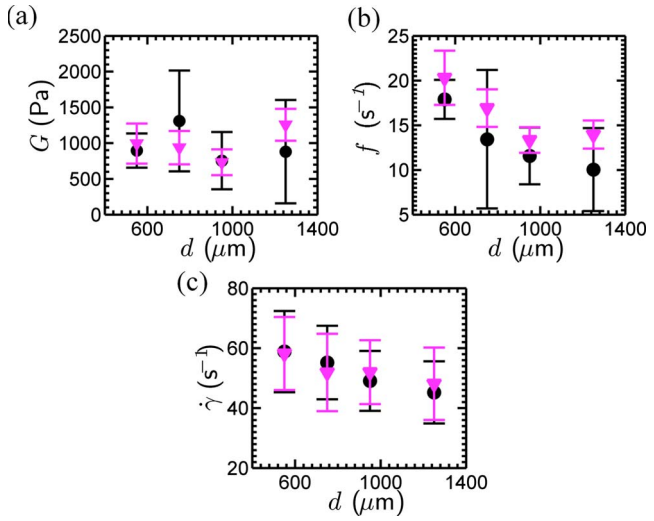

FIG. 10. (Color online) Statistics of flow parameters measured during step stress tests at σ=400 Pa (black circles, dark error bars) and σ=600 Pa (purple triangles, light error bars), performed at various gap heights, d, on the $S1$ sample at ϕ=0.583. In (a) and (b), the symbols represent average values and the bars represent standard deviations from the four steps applied at each stress level. In (c), flow statistics were obtained from the combined data from all stress steps at a give stress. The symbols represent $\bar{\dot{\gamma}}$ and the bars indicate $\Delta\dot{\gamma}$.

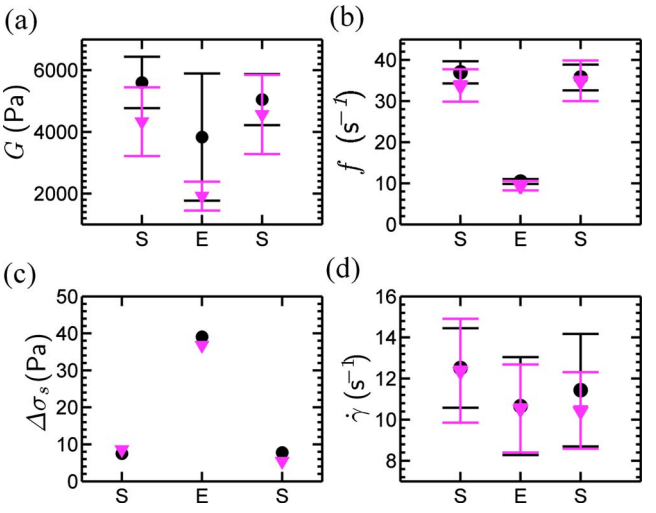

FIG. 11. (Color online) Statistics of flow parameters measured during step stress tests at σ=400 Pa (black circles, dark error bars) and σ=600 Pa (purple triangles, light error bars), on the $D1$ sample at ϕ=0.606. Experiments were performed with standard rheometer inertia (S, at left), then inertia enhanced by a factor of 5.5 (E), then returned to the original rheometer inertia (S, at right). In (a) and (b), the symbols and bars correspond to average values and standard deviations, respectively, calculated from all stress steps at a given stress. In (c) and (d), flow statistics were obtained from the combined data from all stress steps at a given stress. In (d) the symbols represent $\bar{\dot{\gamma}}$ and the bars indicate $\Delta\dot{\gamma}$.

Although our calculations show that G is independent of d, interpretation of this result is complicated by the fact that values of $\bar{\dot{\gamma}}$ are not independent of d, but are higher at lower gap heights [Fig. 10(c)]. This implies that spatial inhomogeneities or slip are present during the measurements. We characterize the gap dependence of $\bar{\dot{\gamma}}$ using a standard slip analysis [24]. Slip causes the apparent shear rate, $\dot{\gamma}$, to be different from the true shear rate, $\dot{\gamma}_{tr}$, according to

$$\dot{\gamma} = \dot{\gamma}_{tr} + 2\frac{V_s}{d}, \tag{5}$$

where V_s is the linear velocity of the upper plate at the outer rim, $V_s = R\dot{\theta}$. Replacing the $\dot{\gamma}$ term in Eq. (5) with $\bar{\dot{\gamma}}$, we perform a least-squares linear fit to the data points at coordinates $(2/d, \bar{\dot{\gamma}})$. From the fit, we take the $\bar{\dot{\gamma}}$ intercept at $2/d = 0$ to be $\bar{\dot{\gamma}}_{tr}$. Calculated values of $\bar{\dot{\gamma}}_{tr}$ are 35 s^{-1} and 41 s^{-1}, for σ=400 Pa and 600 Pa, respectively. These values are 20%–30% lower than the measured values of $\bar{\dot{\gamma}}$. One reason that the presence of slip may not affect the measurements of G is that slip only affects localized dissipation, and it cannot account for elasticity observed during dilatancy.

C. Inertia dependence

If our measurements of G indeed result from an interplay between the sample elasticity and the inertia of the rheometer, then we expect that the time scales associated with the transient fluctuations should depend on I. To test this hypothesis we performed additional experiments in which we modified the inertia of the rheometer.

In these experiments, we increased the rheometer inertia by factors of I_E/I_S=2.1 and 5.5, where the subscript "E" denotes an "elevated" rheometer inertia, and the subscript "S" denotes the standard unmodified inertia. The elevated rheometer inertia was achieved without significantly disturbing the sample by securing circular rings to the shaft of the geometry. The step stress experiments were performed before and after removing the rings to assure that no significant drift occurred in sample properties. The elevated bearing inertia caused samples of lower ϕ to be more likely to exhibit temporary high $\dot{\gamma}$ fluctuations, such as those shown in Fig. 3, especially at the lower σ, such as σ=200 Pa, and sometimes σ=400 Pa. Because an analysis of these fluctuations is beyond the scope of this paper, we limit our analysis to the three experiments at higher ϕ and σ where these events occurred rarely. Under these conditions, values of G measured from $\dot{\gamma}$ transients are lower when I is increased [Fig. 11(a)], corresponding to lower values of f for the larger I [Fig. 11(b)]. Our results indicate that samples appear to be less solidlike when probed with the elevated rheometer inertia. It is tempting to attribute this change to increased yielding of solidlike structures caused by higher inertial stresses. We verified that elevated inertial stresses are present in the sample: increasing I by a factor of 5.5 increases values of $\Delta\sigma_s$ by roughly a factor of four, as shown in Fig. 11(c). If these higher inertial stresses are responsible for breaking down solidlike structures in the sample, then we would expect to observe higher values of $\bar{\dot{\gamma}}$ or $\Delta\dot{\gamma}$. However, our experiments show that both $\bar{\dot{\gamma}}$ or $\Delta\dot{\gamma}$ remain unchanged at elevated I [Fig. 11(d)]. This result is reminiscent of the fact

TABLE I. Average values of G and f calculated from experiments on three samples in which the rheometer inertia was enhanced by a factor of I_E/I_S. This resulted in lower measured values of G, as shown by the fact that $G_S/G_E>1$. Corresponding values of F_S/F_E are intermediate between I_E/I_S and $\sqrt{I_E/I_S}$, implying that both viscous and elastic effects are present.

	$\frac{G_S}{G_E}$	$\frac{I_E}{I_S}$	$\sqrt{\frac{I_E}{I_S}}$	$\frac{f_S}{f_E}$
$S1$, $\phi=0.583$	1.2	2.1	1.4	1.7
$D1$, $\phi=0.606$	1.9	5.5	2.3	3.6
$D1$, $\phi=0.601$	1.7	5.5	2.3	3.4

that $\bar{\dot{\gamma}}$ or $\Delta\dot{\gamma}$ are both independent of the magnitude of the applied stress, σ. A second possible explanation of the lower G values measured at elevated I is that these measurements probe the material response at lower frequencies. A measurement at lower frequency allows more time for the stresses that are stored in the sample to relax.

Step stress experiments with the enhanced inertia were repeated on three samples, which all showed similar trends to those displayed in Fig. 11. For each stress level, we calculate the ratios of f and G values measured with the standard machine inertia, f_S and G_S, to the ratio of those measured with the enhanced inertia, f_E and G_E. Representative values of G_S/G_E and f_S/f_E from each sample were obtained by averaging the values of G_S/G_E and f_S/f_E that were obtained at $\sigma=400$ Pa and $\sigma=600$ Pa. Representative values of G_S/G_E fall between 1 and 2, and values of f_S/f_E were either 1.7 or about 3.5 for $I_E/I_S=2.1$ and 5.5, respectively. These results are shown in Table I.

Our observations also provide evidence that the observed transients do not originate solely from hydrodynamic effects. This is shown with a simple scaling argument from the equation governing the motion of the rheometer. The time scale, τ, associated with the transient shear rates of a Newtonian liquid can be obtained by inserting $\sigma_s \approx \eta\dot{\gamma}$ into the Eq. (1) and is given by $\tau \approx a/\eta$. By contrast, for a Hookean solid, $\sigma_s \approx G\gamma$, and a similar balance with the inertial term yields the scaling, $\tau \approx \sqrt{a/G}$, which is the first-order term of Eq. (4). Therefore, a viscous scaling is given by $\tau_E/\tau_S \propto I_E/I_S$, and an elastic scaling is given by $\tau_E/\tau_S \propto \sqrt{I_E/I_S}$. To check our measurement system, we verified that the expected viscous scaling accurately describes the change in the time scale, τ, associated with the exponential transient responses observed during step stresses on Newtonian liquids, performed at different I. Moreover, we have also verified that our system can accurately measure elastic properties even in the nonlinear regime [22].

Because f is a measurement of the time scale associated with transient effects, we take $\tau=1/f$ and determine whether f_S/f_E is more consistent with an elastic scaling or a viscous scaling. Table I shows that values of f_S/f_E are intermediate between the elastic and viscous scaling, implying the presence of both viscous and elastic effects. To check the appropriateness of interpreting our measured values of f_S/f_E in terms of the scaling argument, we also verify that the observed ratios of f_S/f_E do not depend on the second order correction of Eq. (4), which is not accounted for in the scaling analysis.

IV. DISCUSSION

Taken together, our measurements elucidate the interplay between solidlike and liquidlike behavior at high ϕ during shear thickening. Our most solidlike sample exhibits both elastic recoil and rapid transient ringing. The frequency of the transient ringing continuously decreases with ϕ, causing the apparent flow elasticity, G, to decrease as well. This transition from solidlike to liquidlike behavior characterizes shear thickening at high ϕ. At the most solidlike extreme, $\dot{\gamma}=0$ at $\phi \geq \phi_c$. In such a material, no mechanism exists for stress dissipation, and the material must be an elastic solid [9]. When σ is less than the yield stress, σ_y, of the solid, the applied stresses is stored in the sample. As ϕ descends below ϕ_c at constant σ, σ_y decreases, and the material response to σ transitions from the linear to the nonlinear regime. In doing so, σ transitions from an elastic origin to a viscous origin [15]. As suspensions move through this transition, a smaller proportion of the applied stress is stored and a greater proportion of stress is dissipated. This change is reflected in a decrease in the nonlinear flow elasticity, which we have measured.

In the solid material, stresses less than σ_y are stored in the materials, most likely by particle contacts that percolate through the sample [10]. As ϕ descends below ϕ_c such contacts become unstable due to insufficient crowding of the materials, and this causes flow. Our observation that $\Delta\dot{\gamma}$, is proportional to $\bar{\dot{\gamma}}$ even as ϕ approaches ϕ_c implies that no flow is possible without fluctuations. This leads us to surmise that at elevated σ, flow requires the intermittent breakup of the stress-bearing contacts [13,25,26]. As ϕ decreases at constant σ, the material is less capable of storing elastic stress in the particle contacts, causing G to decrease.

V. CONCLUSIONS

Our studies demonstrate that elastic effects are present during shear thickening and dilatancy at high concentrations. Because the solidlike behavior occurs during flow, we have characterized this elasticity using dynamical measurements that are performed during flow. We have shown that the apparent flow elasticity, G, is an increasing function of ϕ. This is consistent with observations that shear thickening can occur in the context of a jamming transition. We have also shown that G is relatively independent of the gap height, d. These measurements also show that either slip or spatial heterogeneities are present during the experiments. We have shown that values of G decrease as the inertia of the rheometer, I, increases. This may be due to increased yielding due to higher inertial stresses or to structural relaxation due to the fact that measurements with the enhanced inertia probe the material responses at lower frequencies. These measurements demonstrate that the times scales associated with flow fluctuations depend on the inertia of the rheometer and therefore confirm the appropriateness of interpreting the transient

fluctuations in the context of inertio-elastic oscillations.

Although the apparent flow elasticity, G, is useful for describing the relative balance of solidlike and liquidlike behavior in a suspension, it is mean-field time-averaged description of suspension properties. Future work will seek to elucidate the detailed particle-scale mechanisms that are responsible for the observed fluctuations.

ACKNOWLEDGMENTS

This work was supported by the NSF (Grant No. DMR-0602684) and the Harvard MRSEC (Grant No. DMR-0820484) and by the (U.S.) Department of Energy under Award No. DEFG02-91-ER45439 through the Frederick Seitz Materials Research Laboratory at the University of Illinois at Urbana-Champaign.

[1] Y. S. Lee, E. D. Wetzel, and N. J. Wagner, J. Mater. Sci. **38**, 2825 (2003); H. A. Barnes, J. Rheol. (N.Y.N.Y.) **33**, 329 (1989).
[2] W. H. Boersma, J. Laven, and H. N. Stein, AIChE J. **36**, 321 (1990); J. W. Bender and N. J. Wagner, J. Colloid Interface Sci. **172**, 171 (1995); J. Rheol. **40**, 899 (1996); R. S. Farr, J. R. Melrose, and R. C. Ball, Phys. Rev. E **55**, 7203 (1997).
[3] D. R. Foss and J. F. Brady, J. Fluid Mech. **407**, 167 (2000).
[4] M. Lee *et al.*, J. Rheol. (N.Y.N.Y.) **50**, 293 (2006).
[5] P. Hébraud, Rheol. Acta **48**, 845 (2009).
[6] A. Fall, N. Huang, F. Bertrand, G. Ovarlez, and D. Bonn, Phys. Rev. Lett. **100**, 018301 (2008).
[7] D. Lootens, H. van Damme, Y. Hemar, and P. Hébraud, Phys. Rev. Lett. **95**, 268302 (2005).
[8] M. E. Cates, M. D. Haw, and C. B. Holmes, J. Phys.: Condens. Matter **17**, S2517 (2005).
[9] E. Brown and H. M. Jaeger, Phys. Rev. Lett. **103**, 086001 (2009).
[10] C. B. Holmes, M. E. Cates, M. Fuchs, and P. Sollich, J. Rheol. (N.Y.N.Y.) **49**, 237 (2005).
[11] E. Bertrand, J. Bibette, and V. Schmitt, Phys. Rev. E **66**, 060401(R) (2002).
[12] C. B. Holmes, M. Fuchs, and M. E. Cates, Europhys. Lett. **63**, 240 (2003).
[13] J. R. Melrose and R. C. Ball, J. Rheol. (N.Y.N.Y.) **48**, 961 (2004).
[14] J. Mewis and G. Biebaut, J. Rheol. (N.Y.N.Y.) **45**, 799 (2001).
[15] V. T. O'Brien and M. E. Mackay, Langmuir **16**, 7931 (2000).
[16] C. Baravian and D. Quemada, Rheol. Acta **37**, 223 (1998).
[17] G. V. Franks *et al.*, J. Rheol. (N.Y.N.Y.) **44**, 759 (2000); M. E. Fagan and C. F. Zukoski, *ibid.* **41**, 373 (1997); P. D'Haene, J. Mewis, and G. G. Fuller, J. Colloid Interface Sci. **156**, 350 (1993).
[18] R. C. Ball and J. R. Melrose, Adv. Colloid Interface Sci. **59**, 19 (1995).
[19] J. R. Melrose and R. C. Ball, J. Rheol. (N.Y.N.Y.) **48**, 937 (2004).
[20] D. Lootens, H. Van Damme, and P. Hébraud, Phys. Rev. Lett. **90**, 178301 (2003); W. J. Frith *et al.*, J. Rheol. (N.Y.N.Y.) **40**, 531 (1996); H. M. Laun, R. Bung, and F. Schmidt, *ibid.* **35**, 999 (1991).
[21] R. H. Ewoldt and G. H. McKinley, Rheol. Bull. **76**, 4 (2007).
[22] N. Y. Yao, R. J. Larsen, and D. A. Weitz, J. Rheol. (N.Y.N.Y.) **52**, 1013 (2008).
[23] J. W. Kim, R. J. Larsen, and D. A. Weitz, Adv. Mater. **19**, 2005 (2007); A. Donev *et al.*, Science **303**, 990 (2004).
[24] Y. S. Lee and N. J. Wagner, Rheol. Acta **42**, 199 (2003).
[25] M. E. Cates, J. P. Wittmer, J. P. Bouchaud, and P. Claudin, Phys. Rev. Lett. **81**, 1841 (1998).
[26] W. J. Frith and A. Lips, Adv. Colloid Interface Sci. **61**, 161 (1995).